

Investigation of Pseudo-Passivation of Mild Steel in CO₂ Corrosion

Wei Li,* Bruce Brown,* David Young,* and Srdjan Nešić^{†,*}

ABSTRACT

The iron carbonate corrosion product layer formed on mild steel in carbon dioxide (CO₂) environments is known to retard corrosion. When not fully covering the steel surface, it may also lead to initiation of localized corrosion, due to a galvanic effect. In this work, the stability of a protective iron carbonate layer has been studied at 80°C over a relatively wide range of bulk pH. Experiments were done in a glass cell using a three-electrode system. Electrochemical techniques such as linear polarization resistance (LPR) and potentiodynamic polarization (PP) were used. Surface analysis techniques (scanning electron microscopy [SEM], x-ray diffraction [XRD], and transmission electron microscopy [TEM]) were used to confirm the composition and structure of the protective layer. Experimental results confirmed a pseudo-passive behavior, indicated by a positive shift in the open-circuit potential and a significantly retarded corrosion rate for systems at pH 6.0 and above. However, a stable and protective pseudo-passive layer could not be formed at pH 5.6 or lower.

KEY WORDS: CO₂ corrosion product layer, electrochemical techniques, pseudo-passivation, scanning electron microscopy, transmission electron microscopy, x-ray diffraction

INTRODUCTION

Internal carbon dioxide (CO₂) corrosion problems are common in the oil and gas industry. This is because

of the fact that carbon steel is the primary structural material for transportation pipelines, and the aqueous CO₂ environment within the lines has the potential to be corrosive. Although carbon steel has a low cost and a relatively high strength, its corrosion resistance is limited. Use of pH control to provide a more neutral environment and stimulate formation of protective corrosion product layers may leave carbon steel more vulnerable to localized corrosion attack.¹ Despite the fact that the general CO₂ corrosion mechanisms are well understood,²⁻⁵ the role of the protective corrosion product layer and its potential to lead to localized CO₂ corrosion remains unclear.

Iron carbonate (FeCO₃) is a common CO₂ corrosion product found on internal surfaces of mild steel pipelines. As long as Fe²⁺ and CO₃²⁻ are present in the brine at sufficiently high concentrations, which exceed saturation with respect to FeCO₃, precipitation and crystal growth will occur,⁶ according to:



The important threshold is FeCO₃ saturation value (S):

$$S_{(\text{FeCO}_3)} = \frac{C_{\text{Fe}^{2+}} \times C_{\text{CO}_3^{2-}}}{K_{\text{sp}}} \quad (2)$$

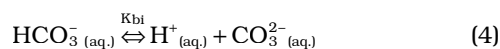
Based on Equation (2), a graph showing the relationship between C_{Fe²⁺}, pH, and S_(FeCO₃) can be constructed (Figure 1). The water chemistry and equilibrium constants that are used for constructing this chart were derived from the literature.⁷⁻¹¹

Submitted for publication: February 19, 2013. Revised and accepted: October 29, 2013. Preprint available online: November 26, 2013. doi: <http://dx.doi.org/10.5006/0950>.

[†] Corresponding author. E-mail: nesic@ohio.edu.

* Institute for Corrosion and Multiphase Technology, Department of Chemical and Biomolecular Engineering, Ohio University, 342 West State St., Athens, OH 45701.

When CO_2 is present in the gas phase, a small fraction of dissolved CO_2 in the water phase forms carbonic acid (H_2CO_3) by hydration.⁷ Carbonic acid can partially dissociate to produce HCO_3^- , H^+ , and CO_3^{2-} in two steps. The reactions for carbonic acid dissociations can be written as:



By writing equilibria expressions for Reactions (3) and (4), one can express the concentration of the $\text{C}_{\text{CO}_3^{2-}}$ as a function of C_{H^+} and $\text{C}_{\text{H}_2\text{CO}_3}$:

$$\text{C}_{\text{CO}_3^{2-}} = \frac{K_{bi}K_{ca}\text{C}_{\text{H}_2\text{CO}_3}}{(\text{C}_{\text{H}^+})^2} \quad (5)$$

For an open system, the $\text{C}_{\text{H}_2\text{CO}_3}$ remains unchanged as long as the CO_2 partial pressure and temperature are given. In that case a simple relation between $\text{C}_{\text{CO}_3^{2-}}$ and C_{H^+} (or pH) can be formulated from Equation (5). When $\text{C}_{\text{CO}_3^{2-}}$ is substituted into Equation (2), a dependency of $S_{[\text{FeCO}_3]}$ on $\text{C}_{\text{Fe}^{2+}}$ and pH is obtained as displayed in Figure 1.

In Figure 1, the line for $S_{[\text{FeCO}_3]} = 1$ divides the area of the graph into two regions: the FeCO_3 supersaturated region on the right and the FeCO_3 undersaturated region on the left. The FeCO_3 supersaturated region on the right ($S_{[\text{FeCO}_3]} > 1$) denotes a condition where there is an excess of Fe^{2+} and CO_3^{2-} ions in solution, and FeCO_3 precipitation prevails over the simultaneously occurring FeCO_3 dissolution (as given by Reaction [1]). In this case, a FeCO_3 layer is expected to form on the steel surface. Conversely, in the FeCO_3 undersaturated region on the left of the line ($S_{[\text{FeCO}_3]} < 1$), the rate of the FeCO_3 dissolution process is faster than the rate of FeCO_3 precipitation, and an FeCO_3 layer cannot form or survive. In Figure 1, the two dotted lines represent the saturation value of 0.5 and 2, outlining a region where relatively small changes in any of the key parameters can make the solution go from an undersaturated to an oversaturated state (or vice versa). It is therefore thought of as an “unstable” region for FeCO_3 and named the “gray zone.” As neither precipitation nor dissolution of FeCO_3 is dominant, this could lead to the metal surface being partially covered by FeCO_3 and a possibility of localized corrosion.

It has been commonly accepted that the FeCO_3 layer is protective because it presents a mass-transfer barrier and slows down the diffusion of cathodic species to the steel surface. However, another effect, direct steel surface coverage, blocking primarily the anodic dissolution of iron, seems to be just as important. Videm and Koren¹² reported a protective effect of corrosion film. Gulbrandsen, et al.,¹³ observed a

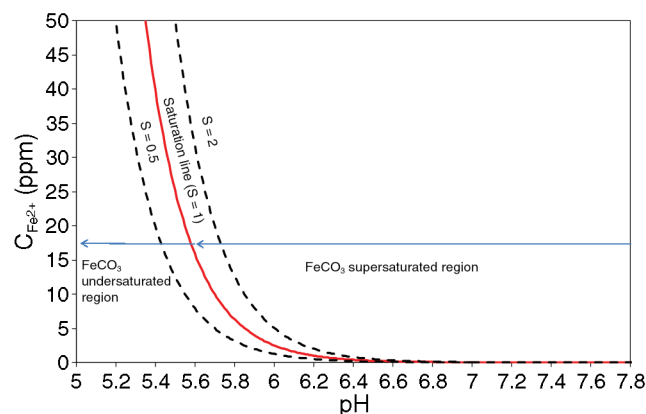


FIGURE 1. Calculation of the dependency of FeCO_3 solubility on $\text{C}_{\text{Fe}^{2+}}$ and pH (80°C , $p\text{CO}_2 = 0.53$ bar (53 kPa), 1 wt% NaCl).

significant increase of open-circuit potential accompanied by a dramatic decrease in corrosion rate in high-pH solutions ($>\text{pH } 7$) when so-called “super-protective” corrosion films formed. Han, et al.,¹⁴ observed similar behavior after the metal surface became fully covered by a FeCO_3 layer, and the corrosion rate reduction was accompanied by a corrosion potential increase—a behavior they termed pseudo-passivation. Han, et al.,¹⁴ hypothesized that the formation of a thin layer of magnetite (Fe_3O_4) under the FeCO_3 layer was the cause of pseudo-passivation. The pH was found to be a critical factor that affects pseudo-passivation. High pH promotes formation of a protective FeCO_3 layer as described above, and promotes pseudo-passivation. Conversely, a decrease in pH will readily lead to a loss of the FeCO_3 layer and the loss of pseudo-passivation. In the “gray zone” the partial coverage/survival by the FeCO_3 layer and the “patchy” pseudo-passive layer may lead to formation of localized galvanic cells and rapid localized attack.¹⁴

The influencing factors and their limits leading to pseudo-passive behavior in CO_2 corrosion are not fully understood.¹⁵ Han, et al.,¹⁴ focused primarily on very high pH ($>\text{pH } 6.6$) in an effort to cause pseudo-passivation to occur more rapidly. Gulbrandsen, et al.,¹³ worked at even higher pH ($>\text{pH } 7$). Very few tests of pseudo-passivation were done in the lower pH range, i.e., at conditions that are more commonly observed in pipelines for oil and gas transportation. In the present study, pseudo-passivation was investigated over a broader, more realistic pH range. Questions about the mechanism of the formation of the corrosion product layer leading to pseudo-passivation, as well as its morphology and chemical composition, are addressed in this paper.

EXPERIMENTAL PROCEDURES

A 2 L glass cell was used for the experiments. A three-electrode system was used for in situ electro-

chemical measurements. Silver/silver chloride (Ag/AgCl) and platinum wire were selected as the reference electrode (RE) and counter electrode (CE), respectively. A cylindrical mild steel specimen (outer diameter 12.0 mm; length 14.4 mm) was used as the working electrode (WE). Additional flat specimens (1.0 cm by 1.0 cm by 0.2 cm) were independently suspended by nylon string in the glass for retrieval during the test to do ex situ surface analyses. Both the cylindrical specimen and flat specimen were made from API⁽¹⁾ 5L X65 steel. For more details about the experimental setup, see the work by Han, et al.¹⁴

Electrochemical measurements using open-circuit potential (OCP) and linear polarization resistance (LPR) were conducted systematically with a potentiostat. The polarization range was ± 5 mV versus OCP and a B value of 26 mV was used. Since an increase in OCP that occurs concurrently with a corrosion rate decrease is considered to be a distinctive indication of a pseudo-passive layer formation,¹⁴ OCP and corrosion rate were monitored continuously during the tests.

Ferrous ion concentration, $C_{\text{Fe}^{2+}}$, in the glass cell was measured ex situ using a UV/visible spectrophotometer and was used to calculate the FeCO_3 saturation value, S_{FeCO_3} , in the system. Scanning electron microscopy (SEM), x-ray diffraction (XRD), grazing incidence x-ray diffraction (GIXRD), and transmission electron microscopy (TEM) were used for sample surface analyses.

The focus of this study was how pH affects the formation of a protective pseudo-passive layer. Consequently, systems with different pH values (from 7.8 to 5.6) were investigated. It should be noted that, in the lower pH range, FeCO_3 is undersaturated in the bulk. To control the FeCO_3 saturation value, S_{FeCO_3} , a deaerated FeCl_2 solution was injected by a syringe into the test system to increase the ferrous ion concentration, $C_{\text{Fe}^{2+}}$.

Before each test, a 1 wt% sodium chloride (NaCl) solution was prepared in the glass cell reactor, deaerated with a continuous CO_2 gas flow purge, and heated to the test temperature by using a hot plate. The test temperature was selected to be 80°C to facilitate a faster formation of the FeCO_3 layer on the steel surface. The tests were conducted at atmospheric pressure. The CO_2 partial pressure was 0.53 bar (53 kPa) at this temperature. After the required temperature was achieved, the bulk pH was adjusted to a designated level and then monitored and maintained during the entire test by addition of sodium bicarbonate (NaHCO_3), sodium carbonate (Na_2CO_3), or dilute hydrochloric acid (HCl) solution (0.1 M) as required.

Both the cylindrical and flat samples were sequentially polished by 400 grit and 600 grit sand paper, and then cleaned in an ultrasonic bath with isopropanol ($[\text{CH}_3]_2\text{CHOH}$). Then, the samples were taken out and dried by nitrogen gas and immediately used for testing in stagnant conditions.

When the samples were removed from the system after test completion, unwanted corrosion product layer oxidation could occur due to exposure to air and affect the subsequent surface analyses. To minimize this effect, samples were taken out and immediately immersed into deaerated deionized water to remove soluble salts on the specimen surface. The sample was then dipped into isopropanol and dried by nitrogen gas, and stored in a vacuum desiccator.

A SEM was utilized to observe the gross surface features of the specimens. Regular XRD and GIXRD analyses were done to examine the chemical compositions of the surface layers. Specimens having shown indications of pseudo-passivation behavior were selected for TEM analysis. Surface cross-sectional samples were prepared by the focused ion beam (FIB) technique. TEM-EDS analysis was performed to obtain the detailed surface morphology as well as compositional information.

RESULTS AND DISCUSSION

Effect of pH on Protective Corrosion Product Layer

As indicated in Figure 1, the pH can significantly influence the saturation state of FeCO_3 , which consequently influences the formation of protective corrosion product layers. Figure 2 shows the OCP and the corrosion rate for tests at different pH values.⁽²⁾ For bulk pH values above 7.0 (high pH), from Figures 2(a) and (b), a significant OCP increase (more than 200 mV) can be observed. At the same time, the corrosion rate is low and stable (less than 0.01 mm/y). This clearly shows that for bulk pH values above 7.0, a stable, protective, pseudo-passive layer has formed in a spontaneous corrosion process without any addition of excess ferrous ions in solution. This can be explained easily by looking at the dependency of FeCO_3 solubility on $C_{\text{Fe}^{2+}}$ and pH (Figure 1). For these pH values, conditions are such that saturation with respect to FeCO_3 is reached even at very low $C_{\text{Fe}^{2+}}$, and the solution will readily become supersaturated as a result of corrosion. A well-developed FeCO_3 layer is expected to form under these conditions and cover the entire carbon steel surface, offering good corrosion protection. Corrosion product layer characterization was done to confirm this and will be discussed in the following section.

For tests at bulk pH 6.6 and 6.0, the formation of a pseudo-passive layer is also indicated in Figures 2(c) and (d), respectively. However, the degree of protectiveness is somewhat lower than for the higher pH

⁽¹⁾ American Petroleum Institute (API), 1220 L Street, NW, Washington, DC 20005-4070.

⁽²⁾ During the experiments, the pH would typically decrease up to 0.5 pH units per day due to precipitation, and this was corrected during the long-term experiments by adding NaHCO_3 to the solution.

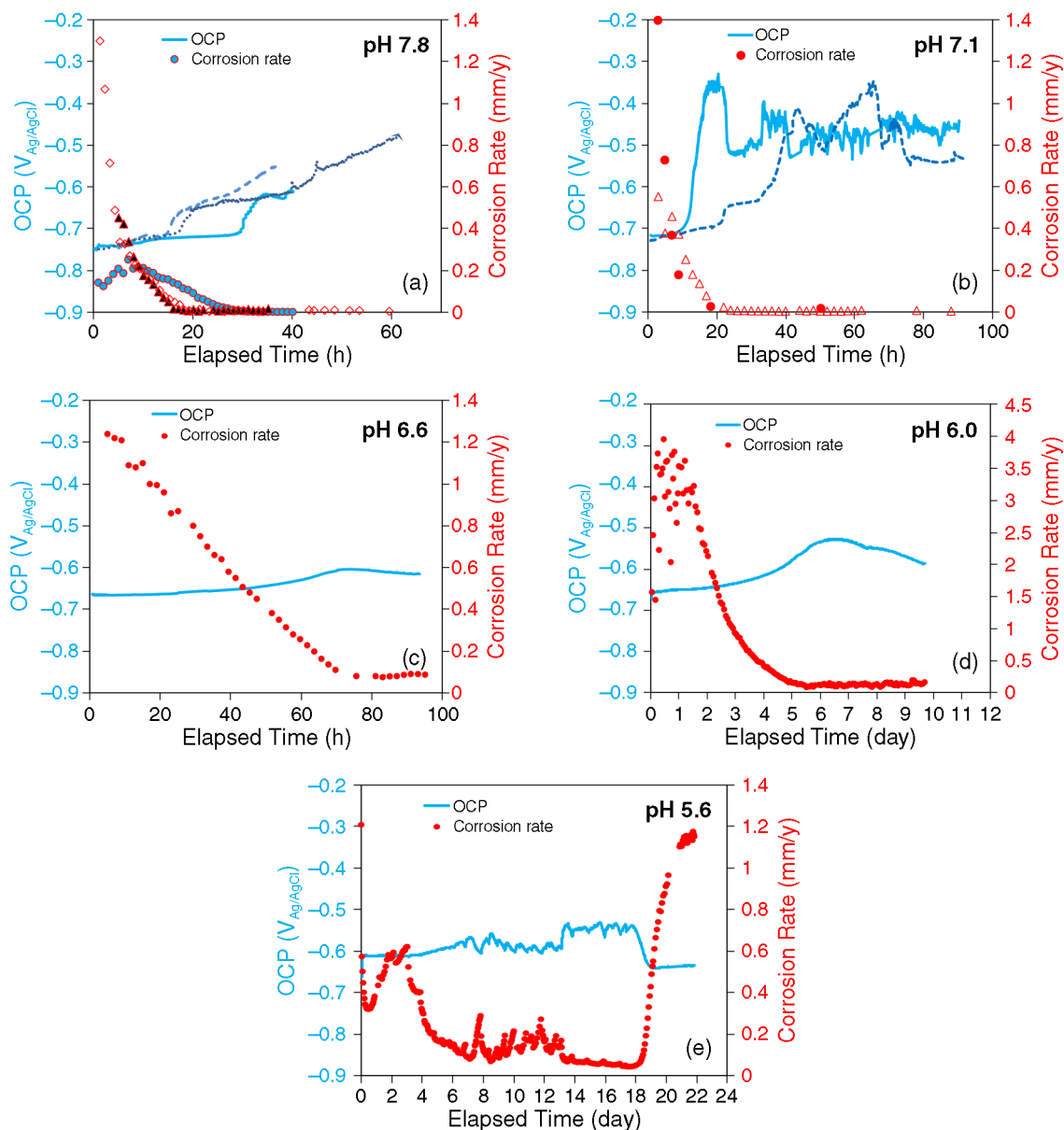


FIGURE 2. Variations of OCP and corrosion rate with time at different pH (80°C, 0.53 bar [53 kPa] CO_2 , 1 wt% NaCl, stagnant): (a) pH 7.8 (two repeats); (b) pH 7.1 (one repeat); (c) pH 6.6 (single experiment), initial $C_{\text{Fe}^{2+}} = 50$ ppm; (d) pH 6.0 (single experiment), initial $C_{\text{Fe}^{2+}} = 100$ ppm; (e) pH 5.6 (single experiment), initial $C_{\text{Fe}^{2+}} = 1,000$ ppm, second $C_{\text{Fe}^{2+}}$ addition at the 13th day to 1,400 ppm. For corresponding SEM images, see Figure 3.

tests. A noticeable OCP increase, less than 100 mV, can still be seen; the final corrosion rate is low, around 0.1 mm/y. In this bulk pH range, the conditions are undersaturated with respect to FeCO_3 formation (without additional ferrous ions present in solution). Therefore, a calculated amount of ferrous chloride was added to the test system to achieve supersaturation and stimulate FeCO_3 precipitation from the bulk solution. It is also necessary to note that the time to form a protective layer in this pH range is longer than for the tests above pH 7. In the pH range of 6.6 to 6.0, it takes more than 3 days before the corrosion rate reaches a low value.

The test at bulk pH 5.6, as shown in Figure 2[e], shows that pseudo-passivation could not be achieved. Neither an OCP increase nor a significant corrosion rate decline can be seen after an extended period of 22 days. Considering the fact that the FeCO_3 is significantly undersaturated in this condition, two large additions of ferrous chloride were made at the 1st and the 13th day of this test (1,000 ppm and 1,400 ppm, respectively) to achieve a high FeCO_3 saturation value. This elevated ferrous ion concentration did initiate precipitation and formation of a corrosion product layer over a period of time (from day 6 to day 18). However, ferrous ions were depleted in the solution

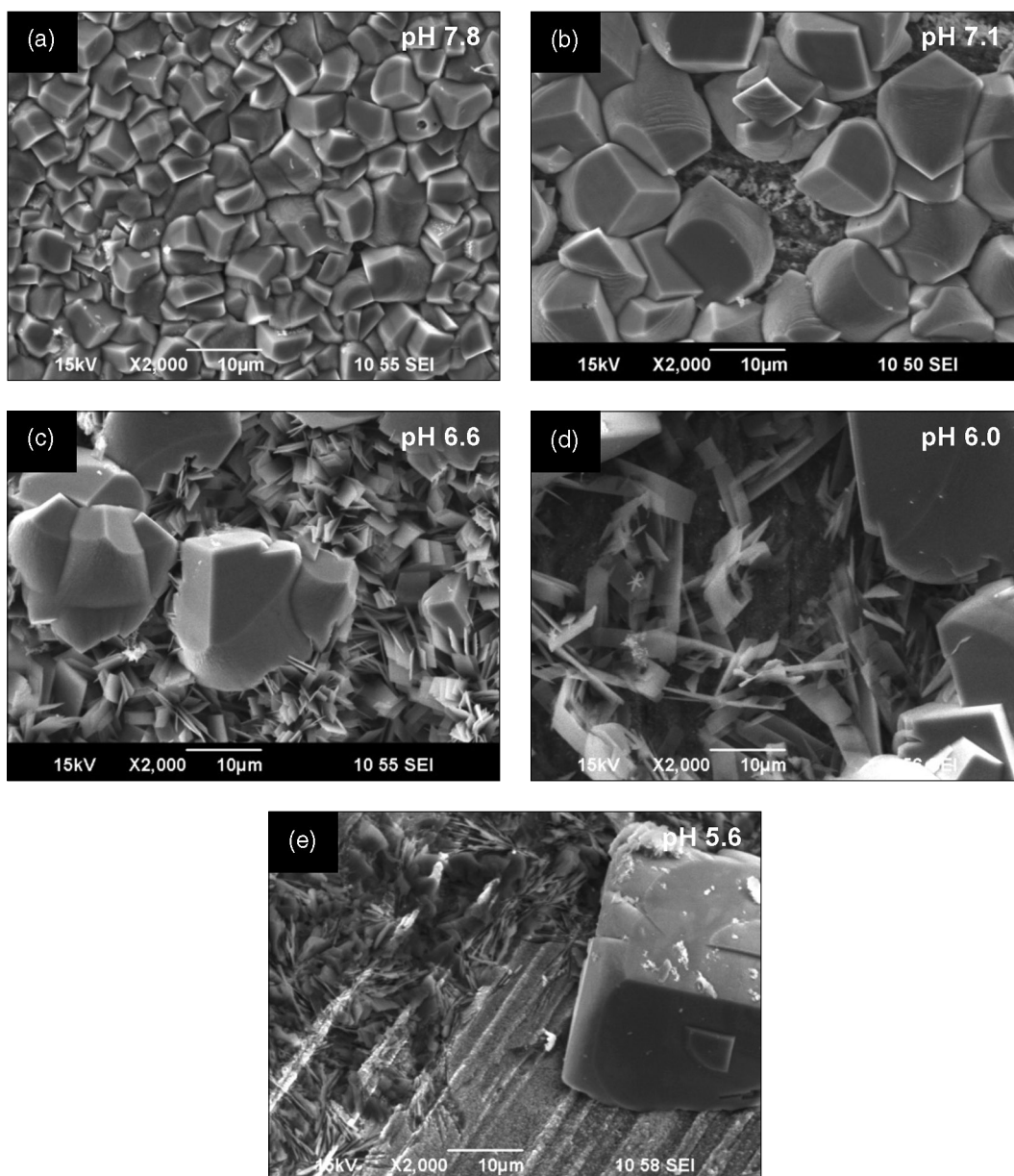


FIGURE 3. Top-view SEM images taken at the end of tests at different pH (80°C, 0.53 bar [53 kPa] CO₂, 1 wt% NaCl, stagnant): (a) pH 7.8; (b) pH 7.1; (c) pH 6.6, initial C_{Fe²⁺} = 50 ppm; (d) pH 6.0, initial C_{Fe²⁺} = 100 ppm; (e) pH 5.6, initial C_{Fe²⁺} = 1,000 ppm, second C_{Fe²⁺} addition at the 13th day to 1,400 ppm. For corresponding corrosion rate/potential images, see Figure 2.

as a result of the precipitation of FeCO₃, and the pH decreased in the process. Eventually, corrosion prevailed and the effect of induced FeCO₃ precipitation vanished.

Morphology and Composition of the Corrosion Product Layers

In Figure 3, SEM images of the samples after each test are shown. They clearly show transitions in surface morphology due to the bulk pH change. At high bulk pH (pH 7.8 and pH 7.1), the FeCO₃ prismatic crystals cover the entire sample surface. At

the intermediate pH values (pH 6.6 and pH 6.0), the dominant morphology of FeCO₃ becomes “platelets,” which would imply a less densely packed and more polycrystalline corrosion product layer structure. A few prism-shaped FeCO₃ crystals were observed. At the low pH value tested (pH 5.6), the steel surface was barely covered with any prismatic FeCO₃. In each case, the main component of this layer was determined by XRD to be FeCO₃.

The dense, prism-shaped FeCO₃ crystals packing on the steel surface at pH 7.8 (Figure 3[a]) offers good corrosion protection (Figure 2[a]). It seems plau-

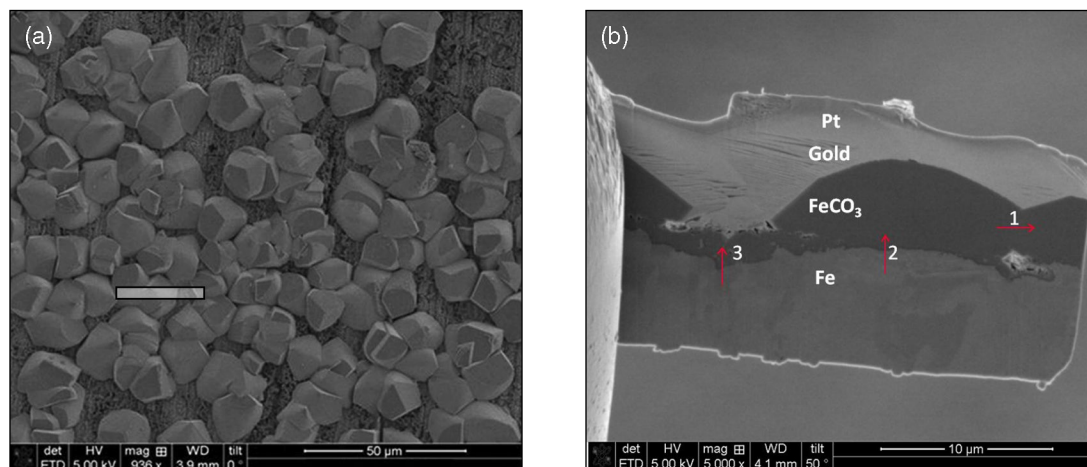


FIGURE 4. TEM images for test conditions of 80°C, 0.53 bar (53 kPa) CO₂, 1 wt% NaCl, stagnant, pH 7.1, after 4 days: (a) top view of TEM sample denoting the cutting area; (b) side view of prepared TEM sample and locations of line EDS scans.

sible to assume that this is because the dense FeCO₃ layer acts as a mass-transfer barrier for the corrosive species. However, for tests at pH 7.1, 6.6, and 6.0, the surface is either not fully covered with densely packed, prism-shaped FeCO₃ crystals or it is covered by loose platelets of FeCO₃. It is difficult to imagine that such a layer can be a significant mass-transfer barrier, which reduces the corrosion rate. However, from Figure 2 it is clear that there is still corrosion protection in these cases. Furthermore, in the test at pH 7.1, the protection is as good as for the test at pH 7.8 while the surface layer does not seem to be nowhere as densely packed. How a seemingly incomplete corrosion product layer can still provide significant corrosion protection cannot be deduced from these SEM images.

Therefore, several cross-sectional samples of the surface layer were prepared to further examine its characteristics. To get appreciable resolution, a TEM was used on a cross-sectional sample produced by FIB. The corrosion product layer produced in the test at pH 7.1 was analyzed, as shown in Figure 4. Outlines of three FeCO₃ crystals can be recognized (seen in the top view as well); however, there is a continuous layer, approximately 2 μm in thickness, beneath them and no “bare” steel surface can be seen. A GIXRD measurement was made to obtain the phase identity information of this sample and is shown in Figure 5. Only FeCO₃ can be identified on the surface. Several EDS scans, plotting the elemental changes along a line (Figure 6), were conducted to investigate the chemical composition at the boundary of the two large FeCO₃ crystals and at the interface between Fe and FeCO₃, in an attempt to detect any minor phases. The scan locations and directions are marked by red arrows and numbered in Figure 4(b). There is no direct indication of any phases other than Fe and FeCO₃ existing on the surface.

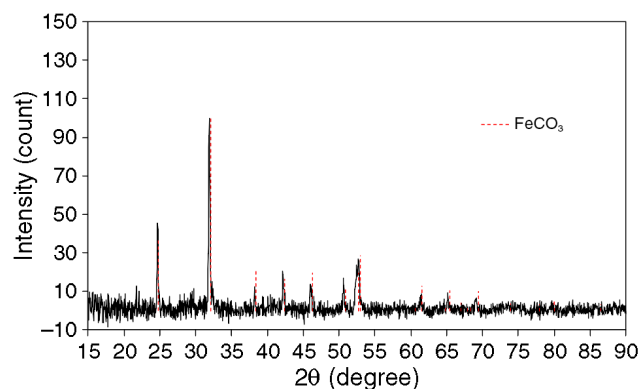


FIGURE 5. GIXRD pattern of X65 flat sample (80°C, 0.53 bar [530 kPa] CO₂, 1 wt% NaCl, stagnant, pH 7.1, after 4 days).

Similar surface analyses have been applied to specimens from other tests. The cross-sectional and XRD results for the test at pH 6.0 are shown in Figure 7. A FeCO₃ layer is still seen to exist beneath the plate-shaped crystals at the surface. In this condition, a new phase, chukanovite (Fe₂[CO₃][OH])₂, was also identified (powder diffraction data for FeCO₃ and Fe₂[CO₃][OH])₂ can be found in the American Mineralogist Crystal Structure Database¹⁶ with code numbers 0000101 and 0007252, respectively). For the test at pH 5.6, which has shown no corrosion protection, cross-sectional and XRD analyses were also made, as shown in Figure 8. No continuous FeCO₃ layer can be seen from the cross section, and the XRD indicates that iron is dominant. Trace amounts of FeCO₃ and Fe₂(CO₃)(OH)₂ were also identified.

The correlation between the surface morphology and pseudo-passivation was investigated. Anodic potentiodynamic polarization was carried out at the end of each test at pH 7.1 with different test durations using the RCE samples; flat samples were also taken

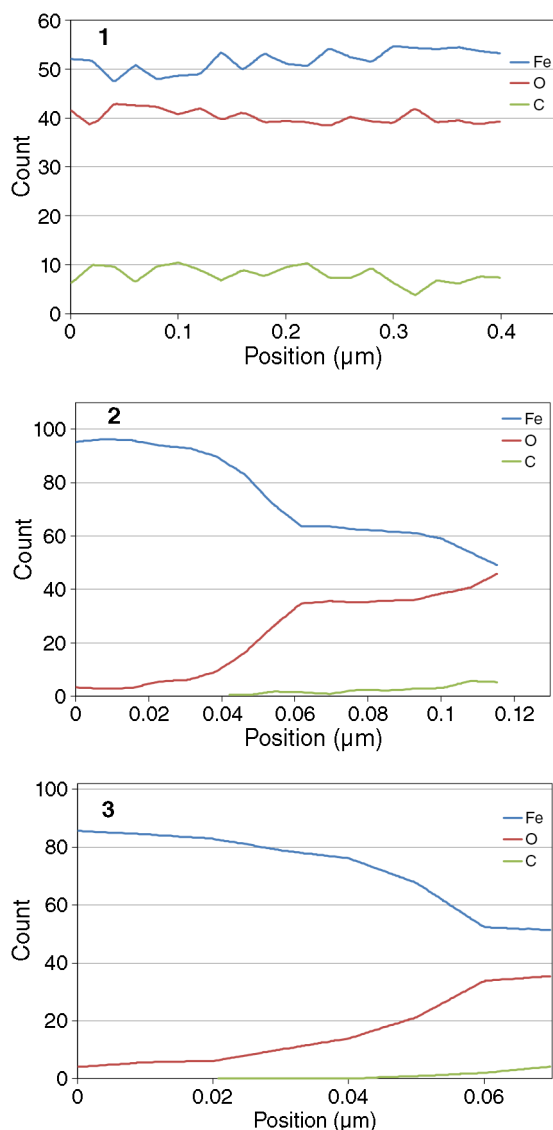


FIGURE 6. Line pattern EDS scan result of locations 1, 2, and 3 shown in Figure 4.

out simultaneously for surface analysis. The results, which are shown in Figure 9, clearly show that with the increase of FeCO_3 coverage, the layer has a more protective nature, noted by significant corrosion current decrease, and, eventually, pseudo-passivation can be achieved. For tests with 1 h and 12 h durations, the steel surface is only partially covered with corrosion product layers, and an active corrosion current peak can still be seen from Figure 9. However, for the test with a 96 h duration, the pseudo-passivation had already happened, which is confirmed with the electrochemical results from Figure 2. Hence, no active corrosion current peak can be seen from the anodic potentiodynamic polarization because the sample steel surface is in the passive state with significantly lower corrosion current.

[†] Trade name.

DISCUSSION

Iron carbonate precipitation is seen when the saturation level of the solution is exceeded. This will more readily occur at the surface of the corroding steel where the concentration of ferrous ions, $C_{\text{Fe}^{2+}}$, and the pH are both higher than in the bulk. Han, et al.,¹⁷ reported that a higher surface pH, compared to bulk pH, was measured in similar CO_2 corrosion systems. In addition, a surface pH with approximately 0.5 to 1 pH units higher than bulk conditions is also predicted by an in-house mechanistic corrosion model (Multicorp[†] V4). A protective FeCO_3 layer formed in the present experiments at pH 6 and above simulations show, however, that this “threshold” pH is lower when the CO_2 partial pressure is higher and at higher temperature.

The protectiveness of the FeCO_3 layer is usually associated with its thickness and porosity, as seen in the SEM images. It is common to assume that the protectiveness of a layer is due to the mass-transfer resistance, which, in this case, a dense and thick FeCO_3 layer offers against inward diffusion of corrosive species. The present experiments have shown that this is only partially correct. For example, good protection was also seen in experiments where the FeCO_3 layer was not dense or thick. Furthermore, the OCP increased when a protective FeCO_3 layer formed, which is the opposite of what is expected when a cathodic reaction is slowed down because of a diffusion limitation (as previously noted by Gulbrandsen, et al.¹³).

It was discovered that a thin ($\sim 1 \mu\text{m}$), adherent “inner layer” forms, which seems to be the key to corrosion protection. In the experiments conducted here, this layer was found to be FeCO_3 . In other studies,¹⁴ at higher pH and temperature, magnetite (Fe_3O_4) was also found in this inner layer. It is highly possible that minor compositional metal phases of X65 carbon steel or other minor iron oxide phases, which are not found by the surface analysis herein, still exist in this corrosion product layer. Those minor phases significantly change the electrical conductivity of the FeCO_3 corrosion product layer. This is indirectly evidenced by the SEM images shown in Figure 3 above. During the SEM specimen preparation, no conductive coating was applied to the specimens. If the surface is only covered by FeCO_3 , which is a low-conductivity material, low-quality SEM images or specimen charging would be expected. On the contrary, the image quality is not affected and no specimen charging is observed, which suggests that the sample is electrically conductive.

Regardless, the protectiveness of this thin layer seemed to be associated with its adherence to the steel surface as much as it was related to its composition. Given the rise in OCP when protective corrosion product layers form in CO_2 corrosion, it was deduced

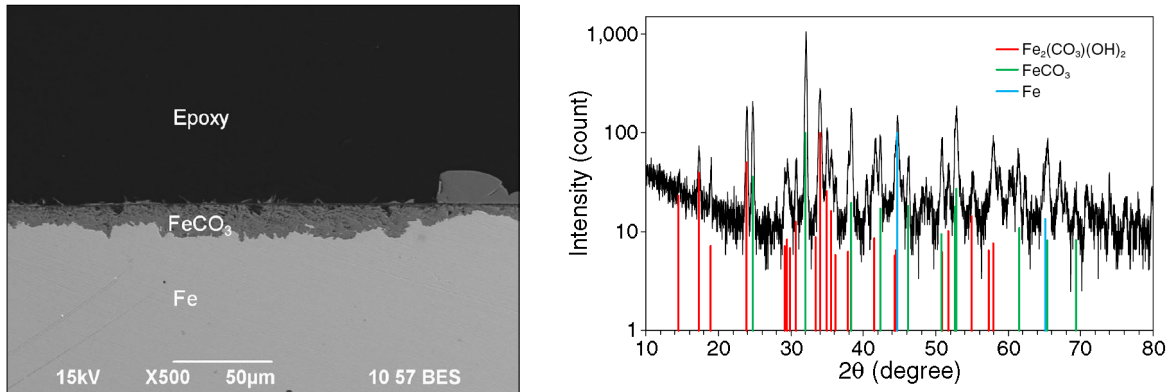


FIGURE 7. SEM cross section and XRD pattern of X65 sample (80°C, 0.53 bar [53 kPa] CO₂, 1 wt% NaCl, stagnant, pH 6.0, initial C_{Fe²⁺} = 100 ppm, after 10 days).

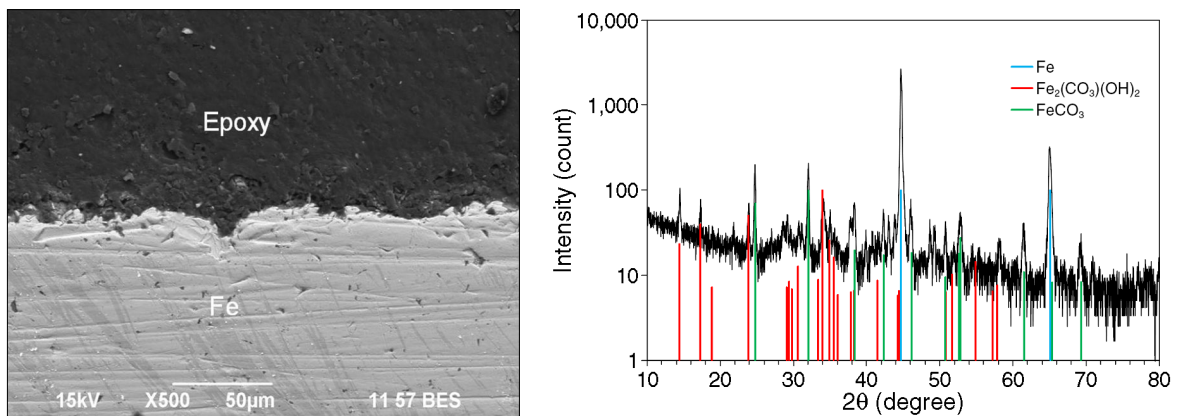


FIGURE 8. SEM cross section and XRD pattern of X65 sample. 80°C, 0.53 bar (530 kPa) CO₂, 1 wt% NaCl, stagnant, pH 5.6, initial C_{Fe²⁺} = 1,000 ppm, after 22 days.

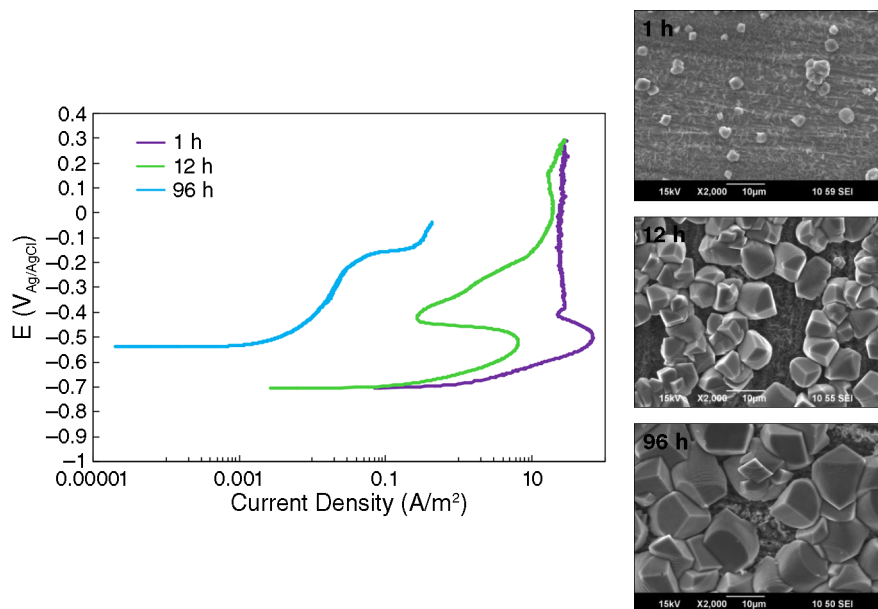


FIGURE 9. Anodic potentiodynamic polarization in the end of each test at pH 7.1 with different test durations and the corresponding surface morphology (80°C, 0.53 bar [53 kPa] CO₂, 1 wt% NaCl, stagnant, potentiodynamic polarization scan rate: 0.1667 mV/s).

that the protection comes from the retardation of the anodic reaction more than the cathodic reaction. Therefore, it is speculated that the thin, adherent corrosion product layer covers/blocks large portions of the steel surface, thereby directly retarding anodic dissolution of iron, which manifests itself as a rise in OCP. It can be speculated that the cathodic reaction, hydrogen evolution, is not affected as much by this layer since the electron path from the steel surface through the corrosion product layer is available due to the presence of minor phases, making it an electronic conductor. The simultaneous reduction of the corrosion rate and increase in the OCP are similar to the classical definition of passivity; however, this behavior is different. The inner layer that forms is still "macroscopic" (visible in SEM and TEM) and the effect is reversible, i.e., the layer is readily removed in under-saturated (typically more acidic) solutions along with its passive-like protection. Therefore, the term that is used here was pseudo-passivity.

There is a role of mass transfer in this scenario. The "outer," more porous FeCO₃ layer, which forms first, does retard the diffusion of corrosive species to the surface but also the diffusion of ferrous ions away from it. This leads to a very different water chemistry at the corroding steel surface when compared to the bulk, where the ferrous ion concentration is much higher and so is the pH, both facilitating formation of the thin, adherent, and more protective pseudo-passive layer.

CONCLUSIONS

The pH effect on protective corrosion product layer formation in mild steel CO₂ corrosion has been studied. Tests at 80°C, with pH ranging from pH 7.8 to pH 5.6, have been conducted. Several conclusions can be drawn from the results and discussion presented in this work:

- ❖ In the pH range from pH 7.8 to pH 6.0 (at 80°C, 0.53 bar CO₂), a protective pseudo-passive layer was observed. This layer significantly lowered the corrosion rate with a noticeable OCP increase.
- ❖ The surface analyses of this pseudo-passive layer revealed that it was made from FeCO₃, that it was thin (~1 μm) and very well attached to the steel surface, and worked primarily by directly blocking the anodic iron dissolution reaction.
- ❖ The mass-transfer resistance offered by the much thicker, outer FeCO₃ crystalline layer was not a direct contributor to corrosion protection, as usually assumed. Its role was primarily to create conditions at the steel surface (high ferrous ion concentration and pH), which are favorable for formation of the inner pseudo-passive layer.

- ❖ No stable FeCO₃ layer nor pseudo-passive layer could be formed at pH 5.6 at 80°C and 0.53 bar CO₂.
- ❖ A bulk pH threshold of about pH 6.0 is needed to get a protective corrosion product layer under the conditions studied in this work; however, this threshold would be lower at higher partial pressures of CO₂ and at higher temperatures.

ACKNOWLEDGMENTS

This paper represents an abridged version of the first author's thesis, which was submitted to Ohio University in partial fulfillment of the requirements for the degree of Master of Science. This work was presented at the CORROSION 2013 conference.¹⁸ The work and revision were conducted under the guidance of S. Nešić of the Department of Chemical and Biomolecular Engineering at Ohio University. The work was financially sponsored from the Corrosion Center Joint Industry Project at Ohio University.

REFERENCES

1. J. Han, B.N. Brown, S. Nešić, *Corrosion* 66, 9 (2010): p. 095003-1 to 095003-12.
2. C. De Waard, D.E. Williams, *Corrosion* 31, 5 (1975): p.177-181.
3. L.G.S. Gray, B.G. Anderson, M.J. Danysh, P.R. Tremaine, "Mechanisms of Carbon Steel Corrosion in Brines Containing Dissolved Carbon Dioxide at pH 4," CORROSION/1989, paper no. 464 (Houston, TX: NACE International, 1989).
4. L.G.S. Gray, B.G. Anderson, M.J. Danysh, P.R. Tremaine, "Effect of pH and Temperature on the Mechanism of Carbon Steel Corrosion by Aqueous Carbon Dioxide," CORROSION/1990, paper no. 40 (Houston, TX: NACE, 1990).
5. S. Nešić, J. Postlethwaite, S. Olsen, *Corrosion* 52 (1996): p. 280-294.
6. S. Nešić, M. Nordsveen, R. Nyborg, A. Stangeland, *Corrosion* 59 (2003): p. 489-497.
7. S. Nešić, W. Sun, "Corrosion in Acid Gas Solutions," in *Shreir's Corrosion*, eds. J.A. Richardson, B. Cottis, R. Lindsay, S. Lyon, D. Scantlebury, H. Stott, M. Graham (Amsterdam, The Netherlands: Elsevier, 2010), p. 1270-1298.
8. Y.K. Kharaka, W.D. Gunter, P.K. Aggarwal, E.H. Perkins, J.D. Debraal, "SOLMINEQ.88, a Computer Program for Geochemical Modeling of Water-Rock Interactions," U.S. Geological Survey, Water-Resources Investigations Report, 88-4227, 1988.
9. J.E. Oddo, M.B. Tomson, *J. Pet. Technol.* 34 (1982): p. 1583-1590.
10. D.A. Palmer, R. Van Eldik, *Chem. Rev.* 83 (1983): p. 651-731.
11. W. Sun, S. Nešić, R.C. Woollam, *Corros. Sci.* 51 (2009): p. 1273-1276.
12. K. Videm, A.M. Koren, *Corrosion* 49, 9 (1993): p. 746-754.
13. E. Gulbrandsen, J.H. Morard, J.L. Crolet, "Study of the Possible Mechanisms of Steel Passivation in CO₂ Corrosion," CORROSION/1999, paper no. 624 (Houston, TX: NACE, 1999).
14. J. Han, D. Young, H. Colijn, A. Tripathi, S. Nešić, *Ind. Eng. Chem. Res.* 48 (2009): p. 6296-6302.
15. G. Schmitt, M. Hörstemeier, "Fundamental Aspects of CO₂ Metal Loss Corrosion—Part II: Influence of Different Parameters on CO₂ Corrosion Mechanisms," CORROSION/2006, paper no. 06112 (Houston, TX: NACE, 2006).
16. R.T. Downs, M. Hall-Wallace, *Am. Mineral.* 88 (2003): p. 247-250.
17. J. Han, B. Brown, D. Young, S. Nešić, *J. Appl. Electrochem.* 40 (2010): p. 683-690.
18. W. Li, B. Brown, D. Young, S. Nešić, "Investigation of Pseudo-Passivation Behavior of Iron Carbonate Layer in CO₂ Corrosion," CORROSION/2013, paper no. 02149 (Houston, TX: NACE, 2013).